

Experimental, Monte Carlo simulation and quantum chemical analysis of 1,5-di(prop-2-ynyl)-benzodiazepine-2,4-dione as new corrosion inhibitor for mild steel in 1 M hydrochloric acid solution

M. Sikine¹, H. Elmsellem^{2*}, Y. Kandri Rodi^{1*}, Y. Kadmi^{5,6}, M. Belghiti², H. Steli⁷,
Y. Ouzidan¹, N. K. Sebbar³, E. M. Essassi^{3,4} and B. Hammouti²

¹Laboratoire de Chimie Organique Appliquée, Université Sidi Mohamed Ben Abdallah, Faculté des Sciences et Techniques, Route d'Immouzer, BP 2202 Fes, Morocco.

²Laboratoire de chimie analytique appliquée, matériaux et environnement (LC2AME), Faculté des Sciences, B.P. 717, 60000 Oujda, Morocco.

³Laboratoire de Chimie Organique Hétérocyclique, URAC 21, Pôle de Compétences Pharmacochimie, Mohammed V University in Rabat, Faculté des Sciences, Av. Ibn Battouta, BP 1014 Rabat, Morocco.

⁴Moroccan Foundation for Advanced Science, Innovation and Research (MASCIR), Rabat Design Center, Rue Mohamed Al Jazouli, Madinat El Irfane, Rabat, Morocco.

⁵Université d'Artois, EA 7394, Institut Charles Viollette, Lens, France

⁶ISA Lille, Ulco Boulogne sur Mer, Université de Lille, EA 7394, Institut Charles Viollette, France

⁷Laboratoire mécanique & énergétique, Faculté des Sciences, Université Mohammed Premier, Oujda, Maroc

Received 29 Oct 2016,
Revised 23 Nov 2016,
Accepted 27 Nov 2016

Keywords

- ✓ 1,4-benzodiazepine-2,4-dione;
- ✓ EIS;
- ✓ Corrosion;
- ✓ Electrochemical;
- ✓ DFT;
- ✓ Fukui function;
- ✓ Monte Carlo;

[h.elmsellem@gmail.com/](mailto:h.elmsellem@gmail.com)
youssef_kandri_rod@yahoo.fr

ABSTRACT

A new corrosion inhibitor namely, 1,5-di(prop-2-ynyl)-benzodiazepine-2,4-dione (M1) has been synthesized and its inhibition action on corrosion of mild steel in 1 M HCl has been investigated using electrochemical impedance spectroscopy (EIS), potentiodynamic polarization, and gravimetric methods. The results obtained from above methods reveal that M1 is an excellent inhibitor. It gives a maximum inhibition efficiency of 90% at 10^{-3} M and inhibits corrosion by adsorbing at the mild steel surface. Polarization study suggested that M1 acts as mixed type inhibitor with some cathodic predominance. Quantum chemical parameters such as EHOMO, ELUMO, ΔE , global hardness and softness, electronegativity and fraction of electron transfer (ΔN) were calculated using DFT method to correlate the electronic properties with the adsorption and inhibition behavior of M1.

1. Introduction

Pickling and acid-cleaning solutions need to be inhibited to prevent corrosion damage to the mild steel surfaces being treated, preferably using a green inhibitor [1]. Hydrochloric acid is often used as industrial acid cleaner and pickling acid [2]. Pickling is used to remove scales from the surface and is usually applied prior to hot-dip coating or electroplating [3]. Acid cleaning is a less severe treatment than pickling and is used for final finish of metal surfaces before plating, painting, or storage. Acid solutions of 40–60% vol hydrochloric acid (often containing up to 1% inhibitor) are used at room temperature for removing soil and light rust.

Molecular structure and electronic characteristics of inhibitor molecules are key factors in establishing the adsorption ability of inhibitors on metal surfaces. Most of the effective inhibitors are organic compounds containing N, S, or O atoms in their structures [4, 5]. Organic compounds containing functional electronegative groups and p electrons in triple or conjugated double bonds are usually good inhibitors [6-8]. The inhibiting action of these organic compounds can be ascribed to their interactions with the metal surface via an adsorption process. Most usually, adsorption of organic compounds on the metal surface is proposed to take place

according to one of the following four mechanisms: (1) the charged metal exerts electrostatic attraction to the charged inhibitor molecules, (2) interaction of lone pair electrons of heteroatoms (N, S or O) with the vacant d-orbital of Fe atoms in the metal, (3) interaction of p electrons in aromatic rings with the vacant d-orbital of Fe atoms in the metal and when feasible, (4) a combination of some of the previous mechanisms [9]. Consequently, inhibitors adsorption is dependent on the nature and surface charge of the metal [10]. If the net charge is negative, the adsorption of cations is favoured while adsorption of anions is favoured when the net charge is positive.

Benzodiazepine derivatives are an important in organic chemistry, they have different applications in several areas . They possess biological activities as anxiolytic, [11] anticonvulsant, [12] antitumor, [13] and anti-HIV [14]. The title compound (M1) was obtained in good yield by action of propargyl bromide in excess on 1,5-benzodiazepine-2,4-dione in dimethyl formamide and potassium carbonate, in the presence of a catalytic quantity of tetra-n-butylammonium bromide. The aim of the present study is to evaluate the corrosion inhibition efficiency of mild steel corrosion in 1 M HCl of 1,5-di(prop-2-ynyl)-1H-benzodiazepine-2,4-dione (M1) (Figure 1). The structure of the product obtained is determined from spectroscopic data and elemental analysis.

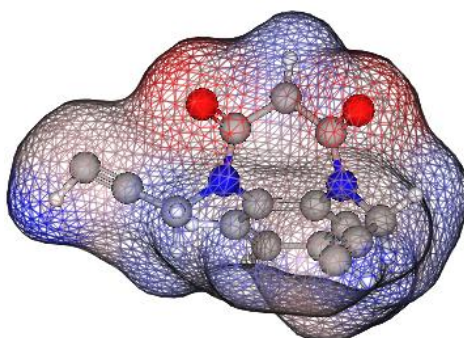


Figure 1. Chemical structure of 1,5-di(prop-2-ynyl)-1H-benzodiazepine-2,4-dione (M1)

2. Experimental section

2.1. Materials and test solution

Mild steel was used for this study has the following composition; Mild Steel strips containing: 0.09 % P; 0.38 % Si; 0.01 % Al; 0.05 % Mn; 0.21 % C; 0.05 % S and the remainder iron as determined by Energy Dispersive Analysis of X-rays (EDAX) method (Figure 2). The specimen was used for electrochemical measurements; the exposed surface area was 1cm². The aggressive solutions of 1.0 M HCl were prepared by dilution of an analytical grade 37% HCl with double distilled water. The concentration range of inhibitor employed was 10⁻⁶ – 10⁻³(mol/L).

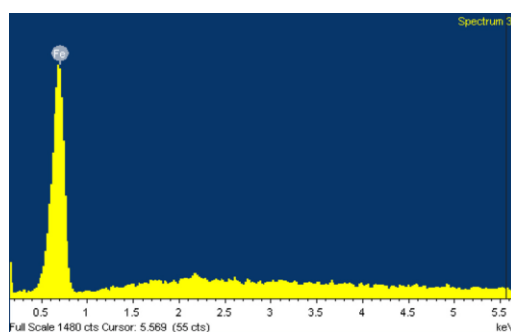
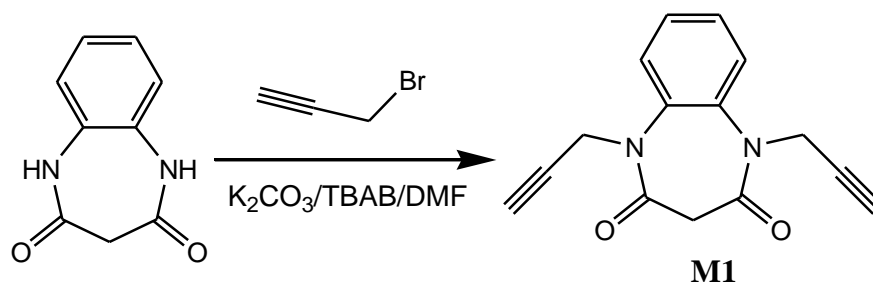


Figure 2. EDX spectrum of mild steel.

2.2. Synthesis of inhibitor

To a solution of 1,5-benzodiazepine-2,4-dione (0.73 mmol), K₂CO₃ (2.19 mmol), tetra-n bromide butyl ammonium (0.1mmol) in DMF (20ml), was added propargyl bromide (1.82 mmol). The mixture was stirred for 6h at room temperature. The solvent was evaporated under reduced pressure, the product is isolated by chromatography on silica gel column with ethyl acetate/hexane (1/3) as eluent. The compound was obtained in 87% yield.



Scheme 1. Synthesis of 1,5-di(prop-2-ynyl)-benzodiazepine-2,4-dione (**M1**).

The analytical and spectroscopic data are conforming to the structure of compound formed:

(M1): Yield: 87%; **M.p**=454K; **RMN¹H** (CDCl₃) **δ ppm**: 2,30 (t, 2H, J = 2,46 HZ, -C≡CH); 3,40 (m, 2H, CH₂C(O)); 4,37 (d, 4H, CH₂-N, J = 2,46); 7,25-7,8 (m, 4H, CH_{ar}). **RMN¹³C** (CDCl₃) **δ ppm**: 37,69 (CH₂-C(O)); 44,19 (N-CH₂); 72,72 (HC≡C); 78,69 (HC≡C); 122,77-127,1 (CH_{ar}); 135,10 (C_q); 164,81 (C=O).

2.3. Corrosion tests

In this work we used the three classical techniques to determine the corrosion inhibitor characteristics of M1 in 1 M HCl medium: The weight loss measurements, electrochemical impedance spectroscopy (EIS) and potentiodynamic polarization curves.

Weight loss testing was developed on rectangular specimens with a size of (1.5 cm × 1.5 cm × 0.1 cm). The immersion time was 6 h at temperature (308 ± 1K) in 1 M HCl solution with and without addition of different concentrations of M1. The weight of each specimen was measured before and after testing using an analytical balance (precision ±0.1 mg). After weighing accurately the specimens were immersed in solutions, at the end of the test, the specimens were taken out, washed carefully and weighed accurately. Triplicate experiments were performed in each case after exposure to 1M HCl solution with and without the addition of various concentrations of M1.

The electrochemical study was carried out using a potentiostat PGZ100 piloted by Voltmaster software. Potentiodynamic polarization measurements were performed in a conventional three electrode cylindrical Pyrex glass cell. The temperature is thermostatically controlled at 308 ± 1K. Mild steel specimen was used as the working electrode, a platinum electrode as the counter electrode and a saturated calomel electrode (SCE) as the reference electrode. The surface area exposed to the electrolyte is 1 cm².

The electrochemical impedance spectroscopy (EIS) measurements are carried out with the electrochemical system (Tacussel), which included a digital potentiostat model Voltalab PGZ100 computer at E_{corr} after immersion in solution without bubbling. After the determination of steady-state current at a corrosion potential, sine wave voltage (10 mV) peak to peak, at frequencies between 100 kHz and 10 mHz are superimposed on the rest potential.

Computer programs automatically controlled the measurements performed at rest potentials after the immersion at 308 K. The impedance diagrams are given in the Nyquist representation. Experiments are repeated three times to ensure the reproducibility.

2.4. Scanning electron microscopy (SEM).

The surface morphology of the sample under study in the absence and presence of inhibitor M1 was carried out using a scanning electron microscope model SU6600 (Serial No: HI- 2102-0003) with an accelerating voltage of 20.0 kV. Samples were attached on the top of an aluminum stopper by means of carbon conductive adhesive tape. All micrographs of the specimen were taken at the magnification of 500x.

2.5. Quantum chemical calculations

Quantum chemical calculations are used to correlate experimental data for inhibitors obtained from different techniques (viz., electrochemical and weight loss) and their structural and electronic properties. According to Koopman's theorem [14], E_{HOMO} and E_{LUMO} of the inhibitor molecule are related to the ionization potential (I) and the electron affinity (A), respectively. The ionization potential and the electron affinity are defined as $I = -E_{\text{HOMO}}$ and $A = -E_{\text{LUMO}}$, respectively. Then absolute electronegativity (χ) and global hardness (η) of the inhibitor molecule are approximated as follows [15]:

$$\chi = \frac{I+A}{2}, \quad \chi = -\frac{1}{2}(E_{HOMO} + E_{LUMO}) \quad (1)$$

$$\eta = \frac{I-A}{2}, \quad \eta = -\frac{1}{2}(E_{HOMO} - E_{LUMO}) \quad (2)$$

Where $I = -E_{HOMO}$ and $A = -E_{LUMO}$ are the ionization potential and electron affinity respectively.

The fraction of transferred electrons ΔN was calculated according to Pearson theory [16]. This parameter evaluates the electronic flow in a reaction of two systems with different electronegativities, in particular case; a metallic surface (Fe) and an inhibitor molecule. ΔN is given as follows:

$$\Delta N = \frac{\chi_{Fe} - \chi_{inh}}{2(\eta_{Fe} + \eta_{inh})} \quad (3)$$

Where χ_{Fe} and χ_{inh} denote the absolute electronegativity of iron atom (Fe) and the inhibitor molecule, respectively; η_{Fe} and η_{inh} denote the absolute hardness of Fe atom and the inhibitor molecule, respectively. In order to apply the eq. 3 in the present study, a theoretical value for the electronegativity of bulk iron was used $\chi_{Fe} = 7$ eV and a global hardness of $\eta_{Fe} = 0$, by assuming that for a metallic bulk $I = A$ because they are softer than the neutral metallic atoms [16].

The electrophilicity has been introduced by Sastri et al. [17], is a descriptor of reactivity that allows a quantitative classification of the global electrophilic nature of a compound within a relative scale. They have proposed the ω as a measure of energy lowering owing to maximal electron flow between donor and acceptor and ω is defined as follows.

$$\omega = \frac{\chi^2}{2\eta} \quad (4)$$

The Softness σ is defined as the inverse of the η [18]

$$\sigma = \frac{1}{\eta} \quad (5)$$

Using left and right derivatives with respect to the number of electrons, electrophilic and nucleophilic Fukui functions for a site k in a molecule can be defined [19].

$$f_k^+ = P_k(N+1) - P_k(N) \quad \text{for nucleophilic attack} \quad (6)$$

$$f_k^- = P_k(N) - P_k(N-1) \quad \text{for electrophilic attack} \quad (7)$$

$$f_k^{\pm} = [P_k(N+1) - P_k(N-1)]/2 \quad \text{for radical attack} \quad (8)$$

where, $P_k(N)$, $P_k(N+1)$ and $P_k(N-1)$ are the natural populations for the atom k in the neutral, anionic and cationic species respectively.

2.6. Molecular dynamic simulation

The Metropolis Monte Carlo (MC) simulations methodology [20] using the DMol³ codes [21] and Adsorption Locator [22] implemented in the BOVIA Material Studio 8.0 (Accelrys, San Diego, CA, USA) [23], has been employed to build the system adsorbate/substrate.

The Monte Carlo simulations (MCs) incorporating molecular mechanics and molecular dynamics were implemented to identify the most stable configuration spacial of inhibitor molecules in isolated form and low configuration adsorption energy of the interactions for single inhibitor molecules on clean iron surface in aqueous hydrochloric acid solution systems.

For the DMol₃ Geometry Optimization, we utilize the (GGA/PW91) function with the DNP+ as basis set for all atoms. This approach makes it possible to obtain the most stable geometry (less energy) of the single inhibitor molecule in isolated form. Simulations were carried out with a slab thickness of 5 Å, a super cell of (7 × 7) and a vacuum of 30 Å along the Cz-axis in a simulation box (35,175 Å × 35,175 Å × 40,266 Å) with periodic boundary conditions to model a representative part of the interface devoid of any arbitrary boundary effects.

For the whole simulation procedure, the COMPASS force field [24] is considered for calculating the interaction forces between different atoms, it was implemented to optimize the structures of all components of the corrosion system (metal substrate / one-inhibitor molecules/ solvent molecules). In order to mimic the real corrosion environment, it is necessary to add some molecules of water in the Monte Carlo Simulation. More detail of Monte Carlo Method is referenced from the published article [25-26].

3. Results and discussion

3.1. Weight loss measurements

3.1.1. Influence of concentration

Table 1 represents corrosion parameters obtained from weight loss data for M1 at different concentrations. Careful inspection of the results revealed that inhibition performance of the M1 increases with increasing its concentrations and maximum inhibition efficiency of 90 % was obtained at 10⁻³M concentration. The increased inhibition efficiency of the M1 on increasing its concentration is attributed to increased surface coverage [27]. The high inhibition efficiency of the investigated M1 at relatively low concentration is attributed to the presence of several heteroatoms in the form of polar functional groups such as prop-2-ynyl, benzo, dione and hetero-aromatic N ring which act as adsorption centers and enhance the inhibition efficiency of the M1 molecule. Furthermore, the presence of polar functional groups such as benzo and dione increases the solubility of the investigated inhibitor which in turn also enhances the effectiveness of the inhibitor molecule.

Table 1. The weight loss parameters obtained for MS in 1 M HCl containing different concentrations of M1.

Inhibitor	Concentration (M)	v (mg.cm ⁻² .h ⁻¹)	E_w (%)	θ
1M HCl	-	0.82	--	--
M1	10 ⁻⁶	0.22	73	0.73
	10 ⁻⁵	0.16	80	0.80
	10 ⁻⁴	0.11	87	0.87
	10 ⁻³	0.08	90	0.90

3.1.2. Adsorption isotherm

Adsorption isotherm is the most important parameter in the field of corrosion study as it provides structural as well as thermodynamic information about electric double layer formed over the metallic surface. Furthermore, adsorption isotherm also gives information about nature and effectiveness of adsorption of inhibitor molecule on the metallic surface. In the present study, the Temkin, Frumkin, and Langmuir adsorption isotherms were tested. The criterion for selection of best isotherm was the value of regression coefficient which was closest to one for Langmuir adsorption isotherm which suggests that the adsorption of M1 on mild steel surface obeyed the Langmuir adsorption isotherm. However, from Langmuir isotherm plot for studied inhibitor shown in Figure 3.

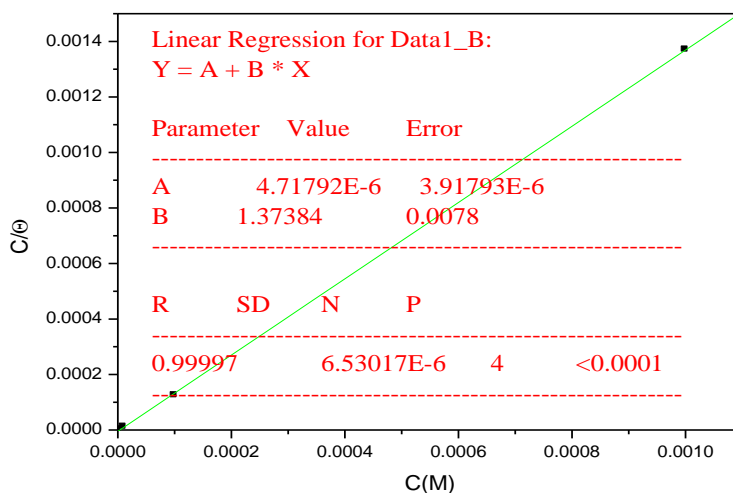


Figure 3. Langmuir isotherm plots for the adsorption of M1 on mild steel surface in 1 M HCl.

it can be seen that the value of slope was much deviated from unity. The deviation from ideal Langmuir adsorption behavior of studied inhibitor molecule might be attributed to intermolecular interactions of the adsorbed inhibitor molecules over the metallic surface which resulted into mutual attraction and/or repulsion [28, 29]. The Langmuir isotherm can be represented by following equation:

$$\frac{\theta}{1-\theta} = K_{ads} C_{inh} \quad (9)$$

where, K_{ads} represents the equilibrium constant for adsorption-desorption processes taking place on the metallic surface, C_{inh} is the concentration and θ is the surface coverage. From the intercept of the Langmuir plot, values of K_{ads} at different studied temperatures were calculated and by employing which values of standard free energy of adsorption (ΔG_{ads}°) were derived using following relationship:

$$\Delta G_{ads}^{\circ} = -RT \ln(55.5K_{ads}) \quad (10)$$

In the above equation, 55.5 denotes the concentration (in mole) of water in acid solution. The derived values of K_{ads} and ΔG_{ads}° at 308K are given in the Table 2. Literature survey revealed that value of ΔG_{ads}° is associated with the nature of adsorption. In general, -20 kJ mol^{-1} or more positive value of ΔG_{ads}° is related with electrostatic interactions between oppositely charged inhibitor molecule and metallic surface [30], and -40 kJ mol^{-1} or more negative value of ΔG_{ads}° is related to electron sharing between inhibitor and metallic surface [31]. In the present case, the values of ΔG_{ads}° is $-41.71 \text{ kJ mol}^{-1}$ indicating that interaction of M1 on mild steel surface in acid solution is the chemisorption [32 – 35].

Table 2. Thermodynamic parameters for the adsorption of M1 in 1 M HCl on the mild steel at 308 K

Inhibitor	Slope	K_{ads} (M^{-1})	$-\Delta G_{ads}^{\circ}$ ($KJ.mol^{-1}$)	R^2
M1	1.37384	2.12E+05	41.71	0.9999

3.1.3. Influence of temperature

Table 3 shows the variation in the values of corrosion rate (w) and percentage inhibition efficiency ($Ew\%$) of investigated inhibitor at its optimum concentration with solution temperature. From the results represented in Table 3, it can be seen that inhibition efficiency of M1 decreases with increasing solution temperature which might be attributed to increased kinetic energy of the inhibitor which decrease the intermolecular force of interaction between adsorbate (M1) and adsorbent (mild steel surface) [36].

Table 3. Variation of w and $E\%$ with temperature in absence and presence of optimum concentration of M1 in 1 M HCl.

Temperature (K)	Corrosion rate (w) ($mg \text{ cm}^{-2} \text{ h}^{-1}$)		$E\%$
	Blank	M1	
308	0.82	0.08	90
318	11.52	1.45	87
328	14.17	2.89	80
338	18.73	6.11	67

Further, molecular rearrangement, rapid etching, and molecular decomposition may also decrease the inhibition performance of the inhibitor [37]. The effect of temperature on the corrosion inhibition efficiency of the M1 can be best represented by Arrhenius equation which represents the natural logarithm of corrosion rate ($\log w$) as a linear function of $1/T$: [38]

$$\log(w) = \frac{-E_a}{2.303RT} + \log \lambda \quad (11)$$

Where, A is the Arrhenius pre-exponent, w is the corrosion rate ($mgcm^{-2} h^{-1}$), T is the absolute temperature and R is the universal gas constant. The slope ($-AE_a/2.303R$) values of Arrhenius plots shown in Figure 4 were employed in order to obtain the values of E_a in the absence and presence of optimum concentration of the studied inhibitor.

The calculated values of E_a were 91 kJ mol^{-1} and 126 kJ mol^{-1} in the absence and presence of M1, respectively. The increased value of E_a in presence of M1 is attributed to increased energy barrier for mild steel corrosion in acid solution in presence of inhibitor [39]. Generally, an organic inhibitor forms surface metal-inhibitor complex which acts as barrier for corrosion process and thereby increases the value of activation energy (E_a) [40].

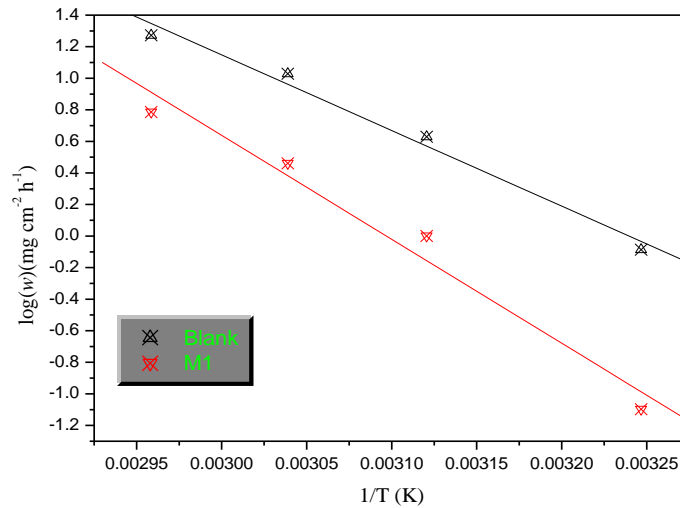


Figure 4. Arrhenius plots for inhibited and uninhibited mild steel specimens in 1 M HCl.

3.1.4. Electrochemical impedance spectroscopy study

The Nyquist and Bode plots for mild steel corrosion in the absence and presence of different concentrations of inhibitor are shown in Figure 5. The Nyquist plots with and without inhibitor consists of a single capacitive loop indicating the charge transfer mechanism which is further supported by a single maxima in the corresponding Bode plots. A careful visualization of the Nyquist plots showed that the diameter of the semicircle capacitive loop increases in presence of increasing concentration of inhibitor. During analysis of Nyquist plots, the difference in the real impedance at lower and higher frequencies is generally termed as charge transfer resistance (R_{ct}).

The inhibition efficiency of the inhibitor was calculated from the charge transfer resistance values using the following equation:

$$E\% = \frac{R_{ct}^{\circ} - R_{ct}}{R_{ct}^{\circ}} \times 100 \quad (12)$$

Where, R_{ct}° and R_{ct} are the charge transfer resistance in absence and in presence of inhibitor, respectively.

Various electrochemical impedance parameters such as solution resistance (R_s), charge transfer resistance (R_{ct}), double layer capacitance (C_{dl}), phase shift (n) and corresponding corrosion inhibition efficiency ($E\%$) were determined with the help of equivalent circuit described elsewhere [41- 42] and are given in the Table 4. Generally, CPE is used in a model at the place of a capacitor to compensate for non-homogeneity in the system. In the present case, impedance of CPE can be represented according to the following equation:

$$Z_{CPE} = \left(\frac{1}{Y_0}\right) [(j\omega)_n]^{-1} \quad (13)$$

In the above equation, Y_0 represents the CPE constant, ω represents the angular frequency, n is the phase shift which provides information about the surface inhomogeneity and j represents the imaginary number. In general, a higher value of n related with lower surface roughness and vice versa. Moreover, the nature of impedance spectra for metal corroding in acid solution can also be explained with the help of n value. For example, $n = 0$ represents the resistance, $n = 1$ represent the capacitance, $n = -1$ represents the inductance and $n = 0.5$ represents the Warburg impedance. In our present study, values of n in the absence and presence of inhibitor molecule range from 0.81 to 0.86. The deviation from unity (ideal capacitive behavior) is attributed to the presence of surface inhomogeneity and surface roughness [43].

The value of double layer capacitance (C_{dl}) can be derived using following equation:

$$C_{dl} = Y_0 [\omega_{max}]^{n-1} \quad (14)$$

where, ω_{max} represents the frequency at which the imaginary part of impedance is maximum (rads^{-1}).

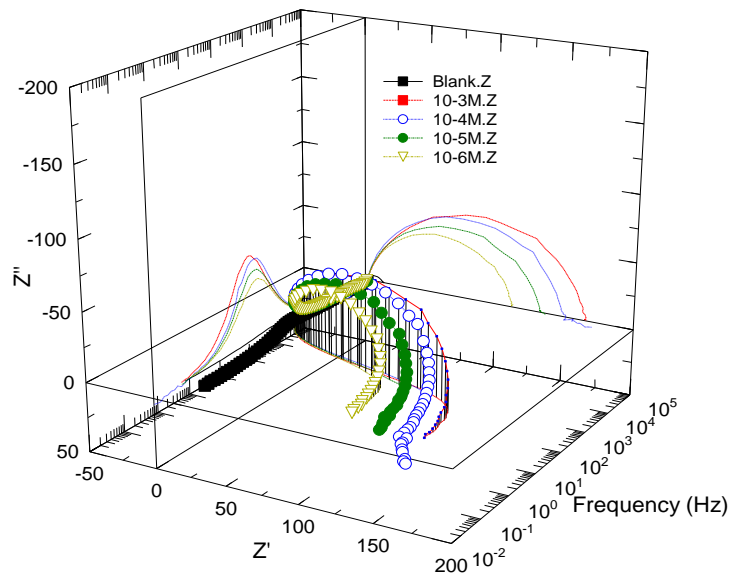


Figure 5. Nyquist, Bode and phase angle plots for mild steel in 1 M HCl in absence and presence of different concentrations of M1.

A careful inspection of the results depicted in the Table 4 shows that the values of R_{ct} increase and that of C_{dl} decrease with increase in the inhibitor concentration which results in an increased thickness of electric double layer due to adsorption of inhibitor molecules on the metallic surface and/or decreased value of dielectric constant due to replacement of water molecules by the inhibitor [43, 44].

The increased surface smoothness in presence of inhibitor can also be supported by Bode plots. The ideal capacitor is characterized by a constant slope value of -1 and phase angle of -90° . However, this deviation from ideal capacitive behavior is attributed to surface roughness [44]. One can see from the Bode plots with and without inhibitor that the deviation from the ideal capacitive behavior is more effective in the absence of inhibitor. The slope and phase angle values significantly increased in presence of inhibitor owing to the formation of a protective film. Moreover, the increased values of phase angles are more effective at high inhibitor concentrations.

Table 4. EIS parameters obtained for mild steel in 1 M HCl at different concentrations of M1 inhibitor.

Parameters	Concentration (M)				
	1M HCl	10^{-6}	10^{-5}	10^{-4}	10^{-3}
Real Center	9.25	57.495	68.109	78.086	84.61
Imag. Center	1.62	12.069	15.889	19.979	20.724
Diameter	15.13	114.01	136.62	158.86	170.41
n	0.81	0.85	0.83	0.86	0.81
Low Intercept R_s ($\Omega.cm^2$)	1.86	1.7825	1.6739	1.2092	1.9658
High Intercept R_t ($\Omega.cm^2$)	16.64	113.21	134.54	154.96	167.25
Depression Angle	12.42	12.224	13.45	14.568	14.077
ω_{max} ($rad s^{-1}$)	929.60	91.169	79.758	74.623	56.04
Estimated R_t ($\Omega.cm^2$)	14.78	111.42	132.87	153.75	165.29
Estimated C_{dl} ($F.cm^{-2}$)	7.11 E-5	6.29E-5	5.17E-5	4.35E-5	4.27 E-5
E (%)	--	87	89	90	91

3.2. Potentiodynamic polarization studies

Polarization measurements have been carried out to pool information concerning the kinetics of anodic and cathodic reaction. Potentiodynamic polarization curves for mild steel in 1N HCl solution in the absence and presence of various concentrations of the inhibitor molecule are shown in Figure 6.

The values of electrochemical kinetic parameters like corrosion current density (I_{corr}) and Tafel slopes (β_a and β_c), determined from these graphs by extrapolation method, are listed in Table 5. The corrosion inhibition efficiency (E_p) was calculated using the relation [45];

$$E_p \% = \frac{I_{corr}^{\circ} - I_{corr}}{I_{corr}^{\circ}} \times 100 \quad (15)$$

Where I_{corr}° and I_{corr} are uninhibited and inhibited corrosion current density respectively determined by extrapolation of Tafel lines in the corrosion potential. In acidic solutions, the anodic reaction of corrosion is the passage of metal ions from the metal surface into the solution, and the cathodic reaction is the discharge of hydrogen ions to produce hydrogen gas or to reduce oxygen. The inhibitor may affect either the anodic or the cathodic reaction, or both. Inspection of Figure 6, shows that the addition of inhibitor has an inhibitive effect on both anodic and cathodic parts of the polarization curves and shifts both the anodic and cathodic curves to lower current densities. This may be ascribed to adsorption of the inhibitor over the metal surface. Therefore, inhibitor M1 can be considered as a mixed type inhibitor.

The cathodic branch of polarization curve gives rise to parallel lines with the increasing inhibitor concentration while cathodic corrosion current density decreased considerably.

This reveals that the addition of M1 does not change the cathodic hydrogen evolution mechanism and the decrease of H^+ ions on the mild steel surface take place mainly through a charge transfer mechanism. The suppression of the cathodic process can be attributed to the adsorption of inhibitor molecules on cathodic sites. Thus, addition of this inhibitor reduces the mild steel dissolution as well as delaying the hydrogen evolution reactions. In the anodic branch of polarization curve the inhibitor molecule first adsorb on the iron surface and blocking the available reaction sites [46]. The surface coverage increases with inhibitor concentration. The formation of surface inhibitor film on mild steel surface reduces the active surface area available for the attack of the corrosive media and delays hydrogen evolution and metal dissolution and provides considerable protection to mild steel against corrosion [47]. The corrosion parameters derived from these curves are listed in Table 5. It is clearly seen that the corrosion current density (I_{corr}) value decrease considerably with increasing concentration of the inhibitor due to the formation of a barrier film on the steel surface, while inhibition efficiency increases with inhibitor concentration, and maximum $E_p\%$ is up to 89 of M1 at $10^{-3}M$.

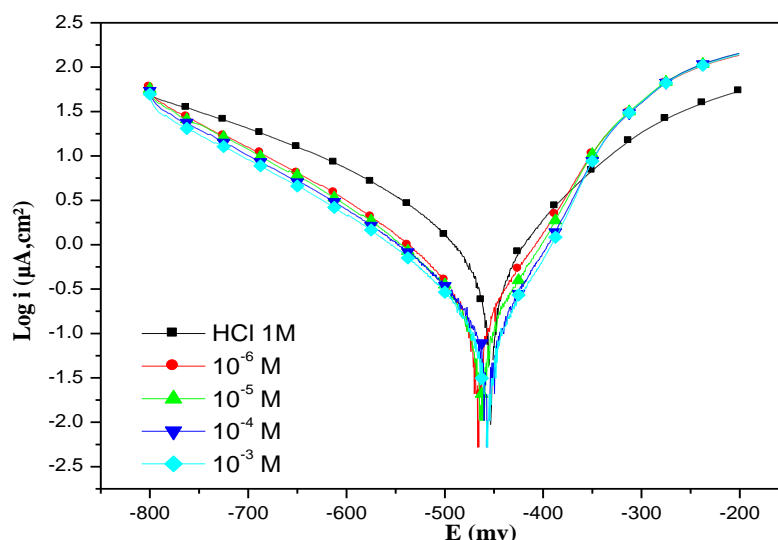


Figure 6. Anodic and cathodic Tafel lines for mild steel in uninhibited 1M HCl and with different concentrations of M1.

Table 5. kinetic parameters calculated from Tafel extrapolation measurements after 30min of immersion in 1M HCl solution with and without inhibitor concentrations at 308K.

Inhibitor	Concentration (M)	E_{corr} (mV/SCE)	I_{corr} (mA cm ⁻²)	β_a (mV dec ⁻¹)	$-\beta_c$ (mV dec ⁻¹)	E_p (%)
Blank	1	-464	1386	113	193	-
M1	10^{-6}	-458	630	101	195	55
	10^{-5}	-460	510	97	172	63
	10^{-4}	-462	349	82	191	75
	10^{-3}	-465	152	74	185	89

3.3. Scanning electron microscopy (SEM)

Surface examination using SEM was carried out to understand the effect of inhibitor molecule on the surface morphology of mild steel. Figure 7a shows the SEM image of a polished mild steel surface. Figure 7b shows SEM image of the surface of mild steel after immersion in acid without inhibitor molecule for 6 h.

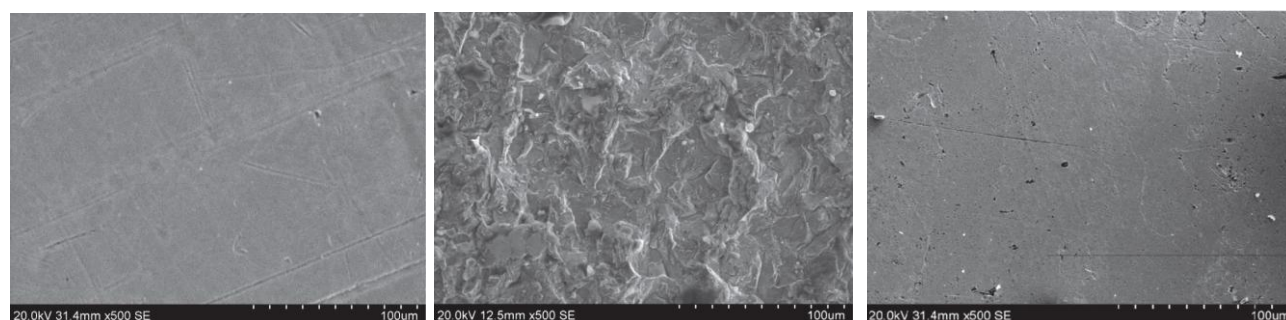


Figure 7. SEM images of (a) blank mild steel, (b) in 1 M HCl without inhibitor, (c) in the presence of 10^{-3} of M1 after 6 h.

This micrograph shows the effect of acid on surface damage. Figure 7c shows SEM image of the surface of mild steel immersed in acid solution containing 10^{-3} of M1. So it can be concluded that corrosion is much less in the presence of inhibitors and the appearance of more polished surface obtained which proves its higher inhibition efficiency.

3.4. Quantum chemical calculations

The FMOs (HOMO and LUMO) are very important for describing chemical reactivity. The HOMO containing electrons, represents the ability (E_{HOMO}) to donate an electron, whereas, LUMO haven't not electrons, as an electron acceptor represents the ability (E_{LUMO}) to obtain an electron. The energy gap between HOMO and LUMO determines the kinetic stability, chemical reactivity, optical polarizability and chemical hardness–softness of a compound [48].

Firstly, in this study, we calculated the HOMO and LUMO orbital energies by using B3LYP method with 6-31G which is implemented in Gaussian 09 packadge [49-50]. All other calculations were performed using the results with some assumptions. The higher values of E_{HOMO} indicate an increase for the electron donor and this means a better inhibitory activity with increasing adsorption of the inhibitor on a metal surface, whereas E_{LUMO} indicates the ability to accept electron of the molecule. The adsorption ability of the inhibitor to the metal surface increases with increasing of E_{HOMO} and decreasing of E_{LUMO} . The HOMO and LUMO orbital energies of the M1 inhibitors were performed and were shown in Table 6 and Figure 8. High ionization energy (> 6 eV) indicates high stability of M1 inhibitor [51], the number of electrons transferred (ΔN), dipole moment, Ionization potential, electron affinity, electronegativity, hardness, Softness and total energy were also calculated and tabulated in Table 6.

Table 6: Quantum chemical parameters for M1 obtained in gas and aqueous phase with the DFT at the B3LYP/6-31G level.

Parameters	Gas phase	Aqueous phase
Total Energy TE (eV)	-22813.1	-22813.6
E_{HOMO} (eV)	-6.8670	-7.1290
E_{LUMO} (eV)	-0.6106	-0.8936
Gap ΔE (eV)	6.2564	6.2354
Dipole moment μ (Debye)	6.3463	8.7603
Ionisation potential I (eV)	6.8670	7.1290
Electron affinity A	0.6106	0.8936
Electronegativity χ	3.7388	4.0113
Hardness η	3.1282	3.1177
Electrophilicity index ω	2.2343	2.5805
Softness σ	03197	0.3207
Fractions of electron transferred	0.5213	0.4793

The value of ΔN (number of electrons transferred) show that the inhibition efficiency resulting from electron donation agrees with Lukovit's study [52]. If $\Delta N < 3.6$, the inhibition efficiency increases by increasing electron donation ability of these inhibitors to donate electrons to the metal surface [53-54].

Pertinent valence and dihedral angles, in degree, of the studied inhibitor calculated at B3LYP/6-31G(d,p) in gas and aqueous phases are given in the table 7.

Table 7 displays the most relevant values of the natural population ($P(N)$, $P(N-1)$ and $P(N+1)$) with the corresponding values of the Fukui functions (f_k^+ , f_k^- and f_k^0) of the studied inhibitors. The calculated values of the f_k^+ for inhibitors are mostly localized on the Benzodiazepinedione ring, namely C_3 , C_6 , C_{11} , C_{12} , O_{16} , N_{17} , N_{18} and O_{19} , indicating that the Benzodiazepinedione ring will probably be the favorite site for nucleophilic attacks.

Table 7: Pertinent natural populations and Fukui functions of M1 calculated at B3LYP/6-31G in gas (G) and aqueous phases.

Atom k	Phase	$P(N)$	$P(N-1)$	$P(N+1)$	f_k^+	f_k^-	f_k^0
C_3	G	6,23713	6,36535	6,23212	0,1282	0,0050	0,0666
	A	6,2368	6,3576	6,22899	0,1208	0,0078	0,0643
C_6	G	6,24493	6,37881	6,23692	0,1339	0,0080	0,0709
	A	6,24325	6,37115	6,23376	0,1279	0,0095	0,0687
C_{11}	G	5,33291	5,39696	5,33729	0,0640	-0,0044	0,0298
	A	5,32266	5,42204	5,31764	0,0994	0,0050	0,0522
C_{12}	G	5,33344	5,4041	5,33876	0,0707	-0,0053	0,0327
	A	5,32248	5,42999	5,31876	0,1075	0,0037	0,0556
O_{16}	G	8,57893	8,66637	8,45337	0,0874	0,1256	0,1065
	A	8,62578	8,70773	8,52344	0,0819	0,1023	0,0921
N_{17}	G	7,44732	7,44885	7,35846	0,0015	0,0889	0,0452
	A	7,44038	7,44977	7,35892	0,0094	0,0815	0,0454
N_{18}	G	7,44926	7,45143	7,36389	0,0022	0,0854	0,0438
	A	7,44689	7,45159	7,35808	0,0047	0,0888	0,0468
O_{19}	G	8,58629	8,66969	8,46078	0,0834	0,1255	0,1045
	A	8,62823	8,70572	8,52321	0,0775	0,1050	0,0913

The geometry of M1 in gas and aqueous phase (Figure 8) were fully optimized using DFT based on Beck's three parameter exchange functional and Lee–Yang–Parr nonlocal correlation functional (B3LYP) [55-56] and the 6–31G. The optimized structure shows that the molecule M1 has a non-planar structure. The HOMO and LUMO electrons density distributions of M1 are given in Table 8.

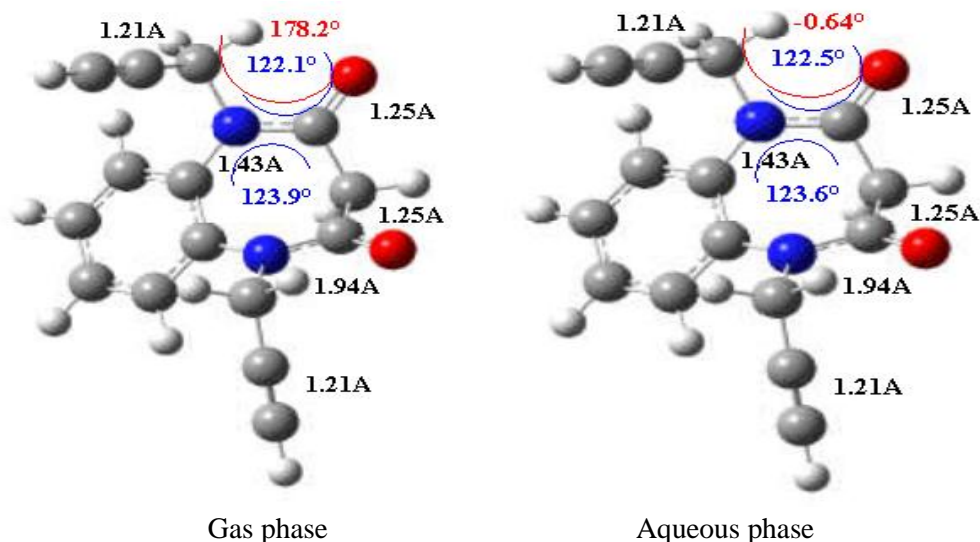


Figure 8: Optimized molecular structures and selected dihedral angles (red), angles (blue) and bond lengths (black) of the studied inhibitors calculated in gaseous and aqueous phases using the DFT at the B3LYP/6-31G level.

As we know, frontier orbital theory is useful in predicting the adsorption centres of the inhibitors responsible for the interaction with surface metal atoms. Table 8 shows the HOMO and LUMO orbital contributions for the neutral studied inhibitor. The HOMO densities were concentrated on Benzodiazepinedione ring.

Table 8. The HOMO and the LUMO electrons density distributions of M1 in gas and aqueous phase computed at B3LYP/6-31G level for neutral forms.

	Gas	Aqueous
HOMO		
LUMO		

3.5. Monte Carlo simulations

In the present study, the atomistic Monte Carlo simulations (MCs) can reasonably predict the most favorable configuration for (single inhibitor molecule (M1) / Fe (111)/100H₂O) system. The optimization energy curve of

single inhibitor molecule (M1) in the neutral and isolated form before putting it on Fe (111) surface has been displayed in Figure 9.

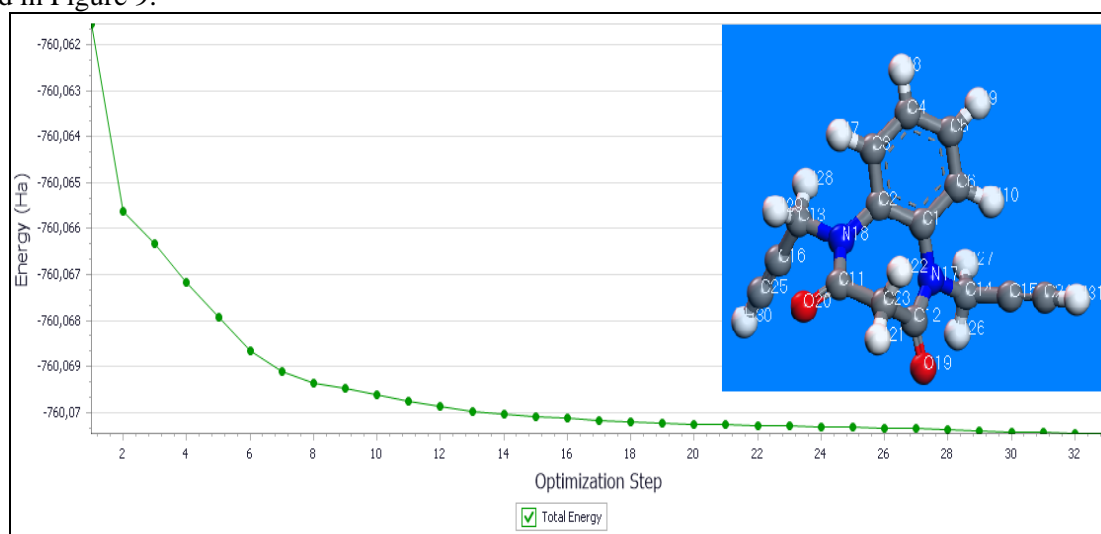


Figure 9. Geometry Optimization of M1-inhibitor in the neutral and isolated forms calculated by DMol3 codes.

In the canonical ensemble, the loading of single inhibitor molecule (M1) onto the Fe (111) surface, as well as the temperature, are fixed. The adsorption energy distribution for system Fe (111)/ (M1) in water solvent molecules obtained by adsorption locator module are shown in Figure 10.

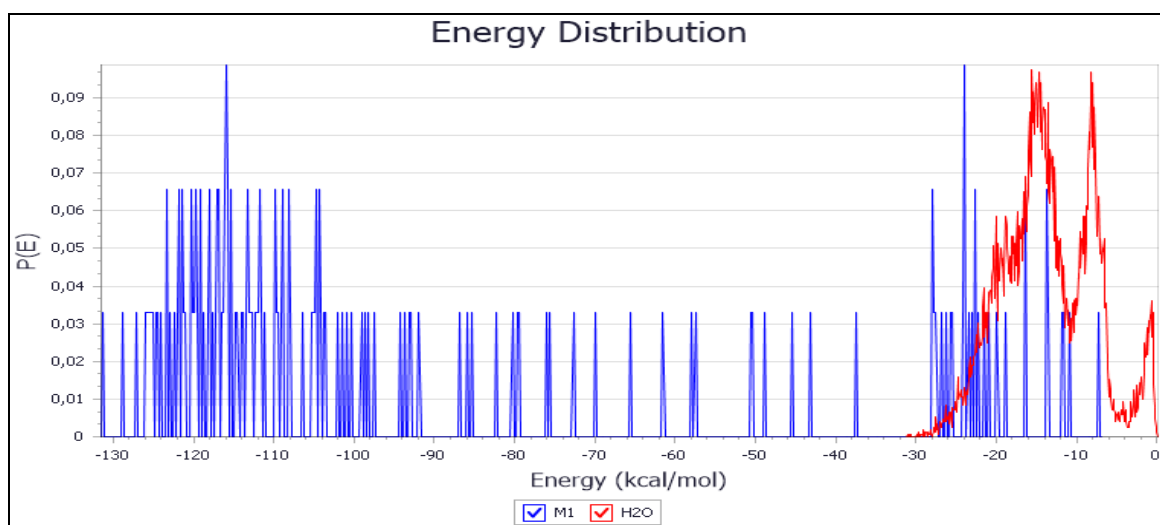


Figure 10. Adsorption energy distribution for Fe (111) / (M1-inhibitor) / 100 H₂O system obtained by adsorption locator module.

As can be seen in Figure.2, the adsorption energy of inhibitor molecule (M1) reaches (-105 Kcal/ mole), which shows the adsorption stronger for Fe (111) / (M1-inhibitor) / 100 H₂O system.

The total energy, Van der Waals energy, average total energy, electrostatic energy and intermolecular energy for the systems under study: Fe (111) / (M1-inhibitor) in water aqueous phase are calculated by optimizing the whole system and given in Figure 11. The most stable low energy adsorption configurations of the inhibitor molecule (M1) adsorbed onto the iron (111) surface in aqueous phase (100H₂O) obtained by adsorption locator module are depicted in Figure 11. Side and top views of stable adsorption configurations for the inhibitors under study on Fe (111) / 100H₂O complex obtained by adsorption locator module has been displayed in Figure 11.

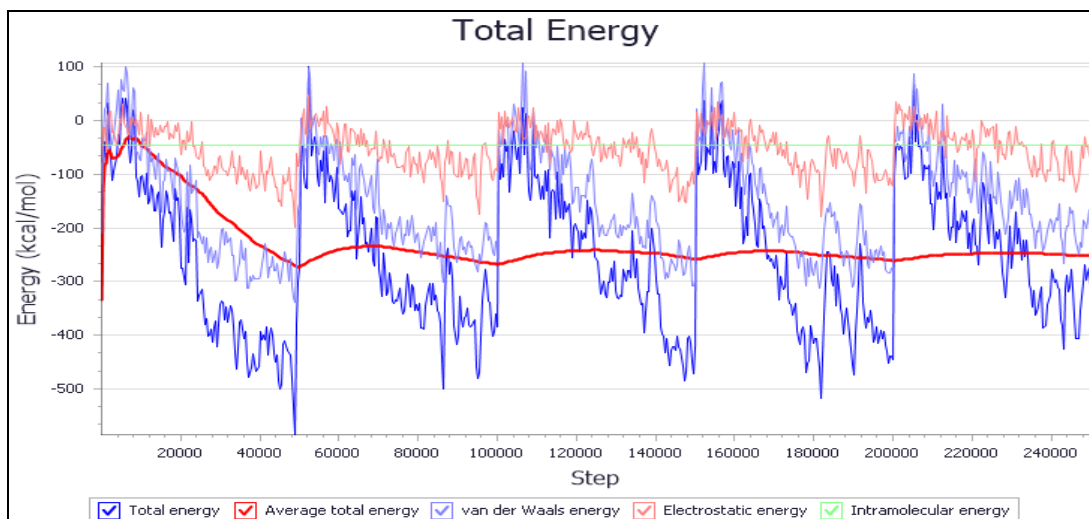


Figure 11. Total energy distribution for Fe (111) / (M1-inhibitor) / 100 H₂O complex during energy optimization process obtained by adsorption locator module.

The most stable (low energy) adsorption configurations of the M1-inhibitor molecule adsorbed onto the iron (111) surface in water solvent molecules (100H₂O) obtained by adsorption locator module are depicted in Figure 11. Side and top views of most stable adsorption configurations of the M1-inhibitor molecule under study on Fe (111) / 100 H₂O system obtained by adsorption locator module as indicated in Figure 12.

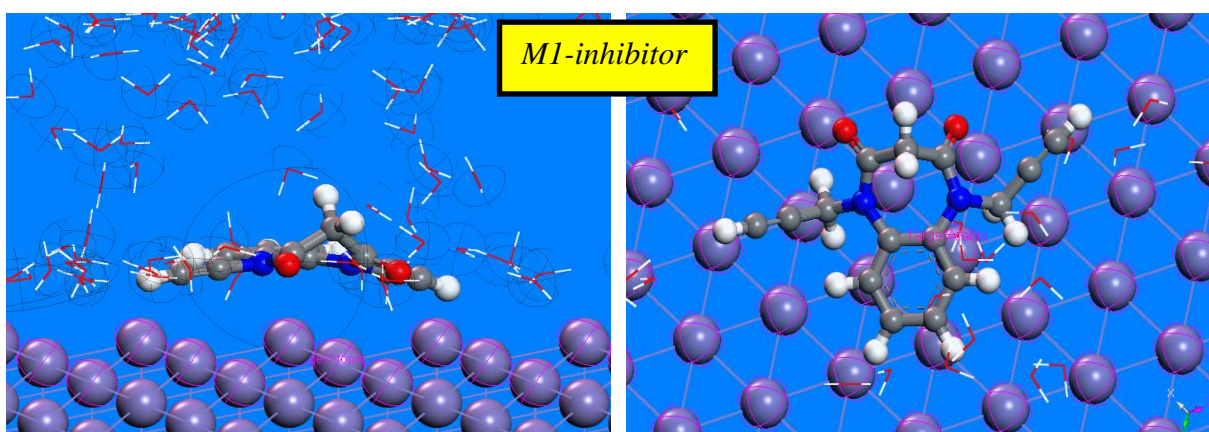


Figure 12. Side and top views of stable adsorption configurations for Fe (111) / M1-inhibitor / 100 H₂O complex obtained by adsorption locator module.

From **Figure 12**, it can be noticed that the adsorption active centers of M1 inhibitor on the Fe (111) surface are the lone pair of the heteroatoms (=N- & -O-) and π electrons of the benzene ring and observed also that the neutral form of single inhibitor molecule (M1) adsorbed nearly parallel onto the Fe (111) surface in water solvent molecules to maximize contact and surface coverage, ensuring a strong interaction between adsorbate and substrate. This is mainly due to the extension of a high inhibition effect observed experimentally. For the inhibitor molecule (M1), the calculated dihedral angles around the benzene ring are close to 0° or 180°, indicating planarity of the benzene ring. Noteworthy, the bond angles between Fe, atoms (-O- or -N=) and (=C-) of Benzodiazepinedione ring after molecular adsorption on iron (111) surface is $\alpha_{\text{Fe-O20-C13}}$: +114.183°, $\alpha_{\text{Fe-O21-C11}}$: +141.03°, $\alpha_{\text{Fe-N18-C1}}$: +73.966° and $\alpha_{\text{Fe-N19-C2}}$: +103.570° (Table 9), which indicate that the inhibitor molecule (M1) are nearly parallel onto the Fe (111) surface in water solvent molecules.

The measured shortest bond distances (**Figure 12**) between the closest heteroatoms (-O- & -N=) of benzodiazepine-dione ring and iron (111) surface at equilibrium were as follows: M1-Fe_{ads} interactions: ($d_{\text{Fe-O20}}$: 2.924Å, $d_{\text{Fe-O21}}$: 2.882Å, $d_{\text{Fe-N18}}$: 3.354Å & $d_{\text{Fe-N19}}$: 2.961Å). Shorter bond distance implies stronger interactions (high inhibition efficiency) [8]. The strong bonding of the heteroatoms of M1 with the Fe atom ensure the chemical nature of the adsorption process (chemisorption). This indicates that the M1 is possible efficient inhibitor. The bond lengths and bond angles of Fe-inhibitor (M1) complex are depicted in Table 9.

Table 9. Bond lengths and bond angles between M1-inhibitor and Fe (111) surface after molecular adsorption.

Bond length	Bond angle
$d_{\text{Fe-O20}}$: 2.924Å	$\alpha_{\text{Fe-O20-C13}}$:+114.183°
$d_{\text{Fe-O21}}$: 2.882Å	$\alpha_{\text{Fe-O21-C11}}$:+141.031°
$d_{\text{Fe-N18}}$: 3.354Å	$\alpha_{\text{Fe-N18-C1}}$:+073.966°
$d_{\text{Fe-N19}}$: 2.961Å	$\alpha_{\text{Fe-N19-C2}}$:+103.570°

The values for the Outputs and descriptors calculated by the Adsorption Locator for Fe (111)/M1/100 H₂O system has been displayed in **Table 10**. The parameters presented in **Table 10** include total energy (E_{Total}), in Kcal/mole, of the substrate/adsorbate system. The total energy is defined as the sum of the energies of all components. In addition, adsorption energy (E_{Ads}), in Kcal/mol, reports energy released (or required) when the relaxed adsorbate component M1 are adsorbed on the substrate (Fe(111)). The adsorption energy is defined as the sum of the rigid adsorption energy (R.A.E) and the deformation energy (D_{Energy}) for the adsorbate components. The rigid adsorption energy reports the energy, in Kcal/mol, released (or required) when the unrelaxed M1 molecule, before the geometry optimization step are adsorbed on the iron (111) surface in presence of 100 molecules of water. The deformation energy (D_{Energy}) reports the energy, in Kcal/mol, released when the adsorbed inhibitor molecule (M1) is relaxed on the iron surface. **Table 10** shows also (dE_{ads}/dN_i), which reports the energy, in Kcal/mol, of Fe–M1 configurations where one of the inhibitor molecule (M1) has been removed.

Table 10. Outputs and descriptors for the lowest adsorption configurations for Fe (111) / (M1) / 100 H₂O system calculated by adsorption locator module. (All values in Kcal/mol).

system	E_{Total}	E_{Ads}	R.A.E	D_{Energy}	dE_{ads}/dN_i Inhs	dE_{ads}/dN_i Water
Substrate	+0.00	--	--	--	--	--
M1-inhibitor	-29.00	--	--	--	--	--
H ₂ O	+0.030	--	--	--	--	--
Fe (1 1 1) - 1	-1168.73	-1142.77	-1181.68	38.91	-105,21	-1.08
Fe (1 1 1) - 2	-1129.41	-1103.45	-1142.25	38.80	-116,65	-0.07
Fe (1 1 1) - 3	-1105.83	-1079.87	-1112.74	32.87	-106,05	-0.21
Fe (1 1 1) - 4	-1102.42	-1076.46	-1102.21	25.74	-108,36	-0.28
Fe (1 1 1) - 5	-1098.68	-1072.72	-1102.06	29.34	-101,74	-0.22
Fe (1 1 1) - 6	-1077.78	-1051.82	-1076.76	24.94	-112,42	-0.57
Fe (1 1 1) - 7	-1062.79	-1036.83	-1068.00	31.17	-121,40	-0.41
Fe (1 1 1) - 8	-1061.38	-1035.42	-1069.75	34.33	-111,49	-0.73
Fe (1 1 1) - 9	-1057.76	-1031.79	-1060.90	29.11	-106,66	-0.37
Fe (1 1 1) - 10	-1056.54	-1030.57	-1058.11	27,53	-101,54	-0.34

It is quite clear from **Table 10** that all adsorption energy values are negative, which denote that the adsorption could occur spontaneously [57]. The large negative values indicate that the Fe.inhibitor (M1) complex is the most stable and stronger adsorption [57]. The adsorption energy value of the M1 (-1168.732 Kcal/mol) in equilibrium configuration, is far higher than that of water molecules (-1,08Kcal/mol). This indicates the

possibility of a progressive replacement of the water molecules from the surface of the iron leading to the formation of a stable layer that can protect the plate against aqueous corrosion.

The result indicates that the inhibitor molecule (M1) has the strongest interaction with the iron surface in Hydrochloric acid solution, which corroborate very well with experimental results.

The adsorption density of inhibitor molecule (M1) on the iron surface has been presented in Figure 13.

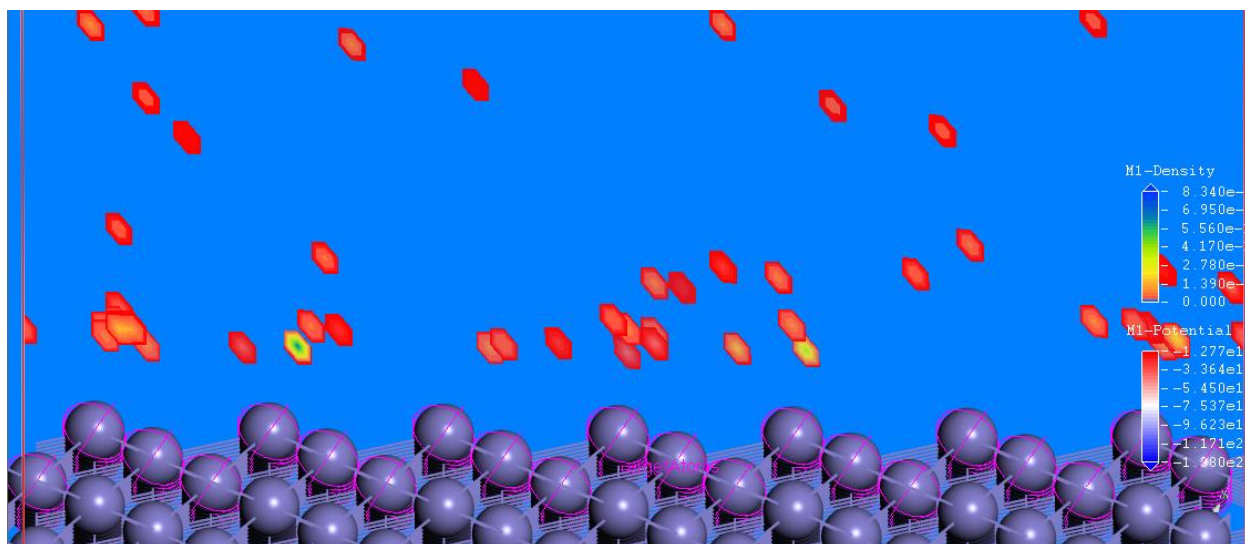


Figure 13. Adsorption density field of M1-inhibitor molecule on the Fe (1 1 1) substrate.

As can be seen from Figure 13 that M1 molecule shows ability to adsorb on the iron surface. In addition, it has high binding energy to Fe surface as seen in Table 2.

Conclusion

From weight loss, electrochemical, surface and quantum chemical studies, it is concluded that the investigated compound acts as a good corrosion inhibitor for mild steel in acid solution and its inhibition efficiency increases with increasing concentration. Maximum inhibition efficiency of 90% was obtained at 10^{-3} M concentration. Adsorption of the compound on mild steel surface obeyed the Langmuir adsorption isotherm. Potentiodynamic polarization study revealed the M1 acted as a mixed type inhibitor with cathodic predominance. EIS results showed that the presence of inhibitor molecule decreased the value of C_{dl} and increased the value of R_{ct} which indicated its adsorption over the metal/electrolyte interface. SEM analyses showed the existence of protective film of inhibitor molecule over the metallic surface. Quantum chemical study confirmed the experimental results and showed that the investigated inhibitor has a strong tendency of adsorption over the metallic surface.

References

1. Mourya P., Banerjee S., Singh M.M., *Corros. Sci.* 85(2014)352–363.
2. Bentiss F., Lagrenee M., Traisnel M., Hornez J.C., *Corros. Sci.* 41(1999)789–803.
3. Elmsellem H., Aouniti A., Toubi Y., Steli H., Elazzouzi M., Radi S., Elmahi B., El Ouadi Y., Chetouani A., Hammouti B., *Der Pharma Chemica.* 7(7)(2015)353-364.
4. Kaddouri M., Bouklah M., Rekkab S., Touzani R., Al-Deyab S.S., Hammouti B., Aouniti A., Kabouche Z., *Int. J. Electrochem. Sci.* 7(2012)9004–9023.
5. Yurt A., Balaban A., Kandemir S.U., Bereket G., Erk B., *Mater. Chem. Phys.* 85(2004)420–426.
6. Elmsellem H., Nacer H., Halaimia F., Aouniti A., Lakehal I., Chetouani A., Al-Deyab S. S., Warad I., Touzani R., Hammouti B., *Int. J. Electrochem. Sci.* 9(2014)5328.
7. Ahamad I., Prasad R., Quraishi M.A., *Corros. Sci.* 52(2010)933–942.
8. Abdel-Gaber A.M., Abd-El-Nabey B.A., Sidahmed I.M., El-Zayady A.M., Saadawy M., *Corros. Sci.* 48 (2006) 2765–2779.
9. Shokry H., Yuasa M., Sekine I., Issa R.M., El-Baradie H.Y., Gomma G.K., *Corros. Sci.* 40 (1998) 2173.
10. Elmsellem H., Basbas N., Chetouani A., Aouniti A., Radi S., Messali M., Hammouti B., *Portugaliae. Electrochimica. Acta.* 2(2014)77.

11. Elmsellem H., Harit T., Aouniti A., Malek F., Riahi A., Chetouani A., Hammouti B., *Protection of Metals and Physical Chemistry of Surfaces*. 51(5) (2015) 873.
12. DeSarro G., Gitto R., Rizzo M., Zappia M., DeSarro A., *General Pharmacology*. 27(1996)935–941. [PubMed: 8909973]
13. Thurston D., Bose D.S, Thompson A.S, Howard P.W, Leoni A, Croker S.J, Jenkins T.C, Neidle S., Hartley J.A, Hurley L.H. *Journal of Organic Chemistry*. 61(199)8141–8147. [PubMed: 11667802]
14. Breslin H.J, Kukla M.J, Kromis T., Cullis H., De Knaep F., Pauwels R., Andries K., De Clercq E., Janssen M.A.C., Janssen P.A.J. *Bioorganic & Medicinal Chemistry*. 7(1999)2427–2436. [PubMed: 10632052]
15. Pearson R.G., *Inorg. Chem.* 27 (1988)734–740.
16. Sastri V.S., Perumareddi J.R., *Corrosion*. 53 (1997)617–622.
17. Pearson R.G., *Inorg. Chem.* 27(1988)734.
18. Sastri, V. and Perumareddi S., *J.R., Corrosion*. 53(1997) 671.
19. Udhayakala P., Rajendiran T. V., and Gunasekaran S., *Journal of Chemical, Biological and Physical Sciences A*. 2(3) (2012)1151-1165.
20. Roy R.K., Pal S., Hirao K., *J. Chem. Phys.* 110(1999)8236.
21. Metropolis N., Rosenbluth AW., Rosenbluth MN., Teller AH., Teller E., *J. Chem. Phys.*, 21 (1953) 1087.
22. Delley B., *J. Chem. Phys.* 113 (2000) 7756.
23. Frenkel D., Smit B., *Understanding Molecular Simulation: From Algorithms to Applications*, 2nd Edition, Academic Press, San Diego (2002).
24. BIOVIA Materials Studio version 8.0, Accelrys Inc. USA., (2014).
25. Sun H., *J. Phys. Chem.* B102 (1998) 7338-7364.
26. Belghiti M. E., Karzazi Y., Dafali A., Obot I.B., Ebenso EE., Emrane KM., Bahadur I., Hammouti B., Bentiss F., *J. Mol. Liq.* 216 (2016) 874-886.
27. Karzazi Y., Belghiti M. E., El-Hajjaji F., Hammouti B., *J. Mater. Environ. Sci.* 7 (10) (2016) 3916-3929.
28. Ramde T., Rossi S., Bonou L., *Int. J. Electrochem. Sci.* 11 (2016) 6819–6829.
29. Larouj M., Lgaza H., Serrard H., Zarroka H., Bourazmib H., Zarroukc A., Elmidaouia A., Guenbour A., Boukhrisd S., Oudda H., *J. Mater. Environ. Sci.* 6 (2015) 3251–3267.
20. Oguzie E.E., Okolue B.N., Ebenso E.E., Onuoha G.N., Onuchukwu A.I., *Mater. Chem. Phys.* 87 (2004) 394–401.
31. Issaadi S., Douadi T., Zouaoui A., Chafaa S., Khan M.A., Bouet G., *Corros. Sci.* 53 (2011) 1484–1488.
32. Elmsellem H., Karrouchi K., Aouniti A., Hammouti B., Radi S., Taoufik J., Ansar M., Dahmani M., Steli H., El Mahi B., *Der Pharma Chemica*, 7(10)(2015)237-245.
33. Chakib I., Elmsellem H., Sebbar N.K., Lahmidi S., Nadeem A., Essassi E.M., Ouzidan Y., Abdel-Rahman I.F., Hammouti B., *J. Mater. Environ. Sci.* 7 (2016) 1866–1881.
34. Elmsellem H., Youssof M. H., Aouniti A., Ben Hadd T., Chetouani A., Hammouti B., *Russian, Journal of Applied Chemistry*. 87(6) (2014)744.
35. Bentiss F., Lebrini M., Lagrenee M., *Corros. Sci.* 47 (2005) 2915–2931.
36. Amin M.A., Ahmed M.A., Arida H.A., Arslan T., Saracoglu M., Kandemirli F., *Corros. Sci.* 53 (2011) 540–548.
37. Elyoussfi A., Elmsellem H., Dafali A., Cherrak K., Sebbar N. K., Zarrouk A., Essassi E. M., Aouniti A., El Mahi B., Hammouti B., *Der Pharma Chemica*. 7(10)(2015)284-291.
38. Verma C., Olasunkanmi L.O., Ebenso E.E., Quraishi M.A., Obot I.B., *J. Phys. Chem. C*. 120 (2016) 11598.
39. Elmsellem H., Elyoussfi A., Sebbar N. K., Dafali A., Cherrak K., Steli H., Essassi E. M., Aouniti A. and Hammouti B., *Maghr. J. Pure & Appl. Sci.* 1(2015)1-10.
40. Khaled K.F., Elhabib O.A., El-mghraby A., Ibrahim O.B., Magdy Ibrahim A.M., *J. Mater. Environ. Sci.* 1 (2010) 139–150.
41. Shukla S.K., Ebenso E.E., *Int. J. Electrochem. Sci.* 6 (2011) 3277–3291.
42. Doner A., Solmaz R., Ozcan M., Kardas G., *Corros. Sci.* 53 (2011) 2902–2913.
43. Solmaz R., Kardas G., Ulha M.C., Yazıcı B., Erbil M., *Electrochim. Acta*. 53 (2008) 5941–5952.
44. Youse A., Javadian S., Dalir N., Kakemam J., Akbari J., *RSC Adv.* 5 (2015) 11697–11713.
45. Verma C., Quraishi M.A., Singh A., *J. Taibah Univ.* 10 (2016) 718–733.
46. Elmsellem H., Aouniti A., Khoutoul M., Chetouani A., Hammouti B., Benchat N., Touzani R. and Elazzouzi M., *J. Chem. Pharm. Res.* 6(2014)1216.
47. Ebenso E.E., Arslan T., Kandemirli F., Caner N., Love I., *Int. J. Quantum Chem.* 110 (2009) 1003–1018.
48. Labjar M., Lebrini N., Bentiss F., Chihib N.E., Hajjaji S.E., Jama C., *Mater. Chem. Phys.* 119 (2010) 330.
49. Govindarajan M., Karabacak M., *Spectrochim Acta Part A MolBiomolSpectrosc.* 85 (2012)251-60.

50. Becke A.D., *J. Chem. Phys.* 98 (1993)1372.
51. Filali Baba Y., Elmsellem H., Kandri Rodi Y., Steli H., AD C., Ouzidan Y., Ouazzani Chahdi F., Sebbar N. K., Essassi E. M., and Hammouti B., *Der Pharma Chemica*, 8(4)(2016)159-169.
52. Elmsellem H., Karrouchi K., Aouniti A., Hammouti B., Radi S., Taoufik J., Ansar M., Dahmani M., Steli H. and El Mahi B., *Der Pharma Chemica*, 7(10)(2015)237-245.
53. Lukovits I., Kalman E., Zucchi F., *Corrosion*, 57(2001)3-7.
54. Sikine M., KandriRodi Y., Elmsellem H., Krim O., Steli H., Ouzidan Y., Kandri Rodi A., Ouazzani Chahdi F., Sebbar N. K., Essassi E. M., *J. Mater. Environ. Sci*, 7 (4)(2016)1386-1395.
55. Elmsellem H., Elyoussfi A., Steli H., Sebbar N. K., Essassi E. M., Dahmani M., El Ouadi Y., Aouniti A., El Mahi B., Hammouti B., *Der. Pharma. Chemica*. 8(1)(2016) 248-256.
56. Lee C., Yang W., Parr R.G., *Phys. Rev.* B37(1988)785.
57. Al Mamari K., Elmsellem H., Sebbar N.K., Elyoussfi A., Steli H., Ellouz M., Y. Ouzidan Y., Nadeem A., Essassi E.M., El-Hajjaji F., *J. Mater. Environ. Sci.* 7(9) (2016) 3286-3299.
58. Ebenso E.E., Kabanda M.M., Arslan T., Saracoglu M., Kandemirli F., Urulana L.C., Singh A.K., Shukla S.K., Hammouti B., Khaled K.F., Quraishi M.A., Obot I.B., Eddy N.O., *Int. J. Electrochem. Sci.*, 7 (2012) 5643-5676.

(2017) ; <http://www.jmaterenvirosci.com/>